



Article

Prediction of Lithium-Ion Battery State of Health Using a Deep Hybrid Kernel Extreme Learning Machine Optimized by the Improved Black-Winged Kite Algorithm

Juncheng Fu ¹, Zhengxiang Song ^{2,3,*}, Jinhao Meng ^{2,3,*} and Chunling Wu ⁴

¹ National Innovation Platform (Center) for Industry-Education Integration of Energy Storage Technology, Xi'an Jiaotong University, Xi'an 710049, China; junchengfu@stu.xjtu.edu.cn

² School of Electrical Engineering, Xi'an Jiaotong University, Xi'an 710049, China

³ State Key Laboratory of Electrical Insulation and Power Equipment, Xi'an 710049, China

⁴ School of Energy and Electrical Engineering, Chang'an University, Xi'an 710064, China; wuchl@chd.edu.cn

* Correspondence: zxsong@mail.xjtu.edu.cn (Z.S.); jinhao@xjtu.edu.cn (J.M.)

Abstract: The accurate prediction of lithium-ion battery state of health (SOH) can extend battery life, enhance device safety, and ensure sustained reliability in critical applications. Addressing the non-linear and non-stationary characteristics of battery capacity sequences, a novel method for predicting lithium battery SOH is proposed using a deep hybrid kernel extreme learning machine (DHKELM) optimized by the improved black-winged kite algorithm (IBKA). First, to address the limitations of traditional extreme learning machines (ELMs) in capturing non-linear features and their poor generalization ability, the concepts of auto encoders (AEs) and hybrid kernel functions are introduced to enhance ELM, resulting in the establishment of the DHKELM model for SOH prediction. Next, to tackle the challenge of parameter selection for DHKELM, an optimal point set strategy, the Gompertz growth model, and a Levy flight strategy are employed to optimize the parameters of DHKELM using IBKA before model training. Finally, the performance of IBKA-DHKELM is validated using two distinct datasets from NASA and CALCE, comparing it against ELM, DHKELM, and BKA-DHKELM. The results show that IBKA-DHKELM achieves the smallest error, with an RMSE of only 0.0062, demonstrating exceptional non-linear fitting capability, high predictive accuracy, and good robustness.

Keywords: lithium-ion battery; state of health; deep hybrid kernel extreme learning machine; improved black-winged kite algorithm



Citation: Fu, J.; Song, Z.; Meng, J.; Wu, C. Prediction of Lithium-Ion Battery State of Health Using a Deep Hybrid Kernel Extreme Learning Machine Optimized by the Improved Black-Winged Kite Algorithm. *Batteries* **2024**, *10*, 398. <https://doi.org/10.3390/batteries10110398>

Academic Editor: Vilayananur Viswanathan

Received: 30 September 2024

Revised: 30 October 2024

Accepted: 6 November 2024

Published: 8 November 2024



Copyright: © 2024 by the authors. Licensee MDPI, Basel, Switzerland. This article is an open access article distributed under the terms and conditions of the Creative Commons Attribution (CC BY) license (<https://creativecommons.org/licenses/by/4.0/>).

1. Introduction

As the energy crisis and environmental issues become increasingly severe, the global demand for green energy continues to rise [1]. Lithium-ion batteries, known for their high energy density, long cycle life, lightweight, and low self-discharge rate, are widely used in portable electronic devices, electric vehicles, and large-scale energy storage systems [2]. However, during long-term use, lithium-ion batteries gradually degrade, manifested by capacity loss, increased internal resistance, and reduced charging and discharging efficiency. This process is known as the degradation of the battery's state of health (SOH). The SOH of a battery is typically used to measure the gap between its current state and its rated state. Estimating SOH is an essential component of battery management systems (BMSs), helping users predict the remaining lifespan of the battery, develop maintenance plans, and even provide early warnings in the event of potential failures [3,4]. In the field of electric vehicles, SOH assessment can impact the estimation of vehicle range and the reuse value of the battery. In renewable energy systems, accurate SOH evaluation is crucial for ensuring the continuous power supply capability of energy storage devices. Therefore, in order to guarantee the safe use of batteries, extend their lifespan, and optimize their operational efficiency, the precise prediction of the SOH is particularly important [5].

1.1. Literature Review of SOH Prediction

SOH prediction methods primarily rely on two types of techniques: model-based methods and data-driven methods [3,6]. Model-based methods include equivalent circuit models, electrochemical models, and empirical degradation models. Reference [7] introduced an empirical degradation model that combines the Verhulst and exponential models. A comparison of this model's fitting performance against exponential models, quadratic polynomial models, and a composite model that combines both revealed that the proposed model is robust and highly flexible; however, it is relatively complex. Reference [8] developed a hybrid prediction model through merging an enhanced particle filter (PF) and a double exponential model. Reference [9] extracted fuzzy entropy as a degradation feature and constructed a non-parametric state space model that describes lithium battery aging characteristics using a metabolic gray model (MGM) and a temporal convolutional network (TCN). SOH prediction was then implemented using the PF model. Reference [10] implemented SOH prediction using a second-order central difference particle filter (SCDPF) combined with a double exponential model. Model-based techniques rely on accurate and complex battery health degradation models. Given that the charging and discharging processes of batteries are viewed as dynamic electrochemical systems, numerous parameters are required to construct such systems, making estimation challenging and hindering the establishment of precise models [11]. Additionally, these models often exhibit poor robustness, leading to estimation errors under varying operating conditions [12,13].

In contrast, data-driven SOH prediction methods predict battery health by analyzing historical operational data using machine learning models. These models do not ask for a grasp of the battery's internal electrochemical principles; instead, they learn the degradation patterns from the data to achieve relatively accurate health assessments [14–16]. Currently, widely used machine learning algorithms include support vector regression (SVR) [17], random forests (RFs) [18], neural networks (NNs) [19], and Gaussian process regression (GPR) [20], all of which have shown promising results. Reference [21] proposed a prediction technique that employs indirect characteristic factors with SVR, optimizing SVR hyperparameters using an improved ant lion optimization algorithm (IALO). This method achieved accurate online health state predictions. Reference [22] introduced a predictive framework that combines data preprocessing with variational mode decomposition (VMD), long short-term memory networks (LSTM), and GPR. The VMD-LSTM approach enabled the decomposition, prediction, and reconstruction of health factors, and the reconstructed data were then applied to the GPR model for health state prediction. Reference [23] utilized a Transformer model for SOH estimation, achieving high accuracy; however, the model exhibits high computational complexity. Reference [24] employed a particle swarm optimization algorithm to enhance the SOH prediction method based on LSTM, but its ability to capture non-linear components is limited, and its computational speed is slow.

As the complexity of battery systems increases, the existing data-driven methods still need improvement in performance and predictive accuracy when dealing with non-linear, high-dimensional lithium battery data. Extreme learning machine (ELM) is an emerging single-hidden-layer feedforward neural network algorithm characterized by its simple structure, fast computation speed, and strong generalization capability [25]. Unlike traditional gradient descent methods, ELM randomly initializes the weights and biases of the hidden layer and then solves for the output weights by minimizing the output error, thus avoiding the cumbersome backpropagation process and significantly accelerating model training. In lithium battery SOH prediction, ELM has garnered increasing attention from researchers due to its rapid learning characteristics and ability to handle non-linear data. Although ELM models have achieved some success in SOH prediction, they still face limitations when dealing with complex battery data [26]. Specifically, ELM is sensitive to parameter selection, which may affect prediction accuracy and the model's generalization ability. Furthermore, the fitting capability of ELM for non-linear data requires further enhancement. Consequently, improving the ELM model and optimizing its parameter

selection to enhance its adaptability under complex operating conditions has become a key focus of current research [27]. Various optimization algorithms provide effective solutions for parameter selection in models. The black-winged kite algorithm, in particular, is known for its fast convergence, strong optimization capabilities, and robustness. Moreover, its improved variants have also shown promising results in fields such as engineering optimization and machine learning [28,29].

1.2. Contribution of the Paper

Inspired by the aforementioned literature, this study proposes a deep hybrid kernel extreme learning machine (DHKELM) optimized by the improved black-winged kite algorithm (IBKA) to enhance the performance of ELM models in lithium battery SOH prediction. We conducted extensive validation using the NASA and CALCE datasets. The main contributions of this paper are as follows:

(1) The concepts of auto encoders and hybrid kernel functions were introduced into the ELM framework. The improved DHKELM significantly enhances performance on non-linear, high-dimensional SOH data. The auto encoder optimizes data input through layerwise feature extraction, making the model more efficient in handling complex non-linear features. Additionally, the high-dimensional mapping capability of the hybrid kernel function further strengthens the model's non-linear mapping ability.

(2) The IBKA was improved by employing an optimal point set strategy, the Gompertz growth model, and a Levy flight strategy. These enhancements address the limitations of the standard BKA.

(3) By combining the improved black-winged kite algorithm with the deep hybrid kernel extreme learning machine, we offer a new solution for predicting the SOH of lithium batteries. This method not only overcomes the limitations of traditional machine learning models in handling high-dimensional non-linear data but also improves both predictive accuracy and generalization capability through the introduction of an optimization algorithm.

The remainder of this paper is organized as follows: Section 2 discusses the lithium battery health state prediction model. Section 3 covers the laboratory dataset and the extraction of aging features. Section 4 presents the experimental results and analysis. Finally, we conclude the paper in Section 5.

2. Lithium Battery State of Health Prediction Model

2.1. Deep Hybrid Kernel Extreme Learning Machine (DHKELM)

2.1.1. Hybrid Kernel Extreme Learning Machine (HKELM)

Traditional ELM only requires setting a quantity of hidden layer nodes to generate the local optimal solution without the need to adjust the weights of the input layer or the biases of the hidden layer. Unlike conventional neural networks, which require extensive parameter tuning for training, ELM offers faster convergence rates and higher learning efficiency [30,31].

The output model of ELM is represented as shown in Equation (1).

$$f(x) = \beta H \quad (1)$$

where H represents the output matrix of the hidden layer nodes, and β denotes the weights between the hidden layer and the output layer, which is calculated using the following equation:

$$\beta = H^+ T \quad (2)$$

where H^+ represents the Moore–Penrose pseudoinverse of the hidden layer output matrix H .

Kernel methods possess strong non-linear mapping capabilities. To enhance the learning and generalization abilities of ELM, different types of kernel functions are combined.

By introducing kernel parameters $\mathbf{H}\mathbf{H}^T$, the generalization capacity of the ELM model is improved, and the output function of KELM can be expressed as follows:

$$f(x) = \mathbf{H}\mathbf{H}^T(\mathbf{H}\mathbf{H}^T + I/C)^{-1}\mathbf{T} \quad (3)$$

where C is a positive constant representing the penalty parameter; I is the identity matrix; and \mathbf{T} is the target output matrix.

The kernel function of KELM is defined as follows:

$$f_{KELM} = \mathbf{H}\mathbf{H}^T; f_{KELM_{i,j}} = h(x_i)h(x_j) = K(x_i, x_j) \quad (4)$$

The model function of KELM can be expressed as follows:

$$f(x) = \begin{bmatrix} K(x, x_1) \\ \dots \\ K(x, x_N) \end{bmatrix} (\frac{\mathbf{I}}{C} + f_{KELM})^{-1} \mathbf{T} \quad (5)$$

Traditional kernel functions include global and local kernel functions. Global kernel functions emphasize the overall influence of data on the kernel, offering strong generalization capabilities but weaker learning ability. In contrast, local kernel functions highlight the impact of data near critical points, exhibiting strong learning capabilities but weaker generalization [27].

The Gaussian kernel function is a local kernel function that outperforms polynomial kernel functions in terms of learning capability. The expression for the Gaussian kernel function is as follows:

$$K_{RBF}(x_i, x_j) = \exp\left(-\frac{\|x_i - x_j\|^2}{2\sigma^2}\right) \quad (6)$$

where σ is the parameter used to control the radial range.

The polynomial kernel function is a global kernel function known for its strong generalization capability, and its expression is as follows:

$$K_{poly}(x_i, x_j) = ((x_i, x_j) + q)^p \quad (7)$$

where q and p represent the constant parameter and the exponent parameter of the polynomial kernel function, respectively.

To enhance the learning and generalization capabilities of KELM, a combination of two kernel functions is proposed as a mixed function. This paper employs a linear weighting method, and the equation for the new mixed function is expressed as follows:

$$K(x_i, x_j) = vK_{RBF} + (1 - v)K_{poly}, v \in [0, 1] \quad (8)$$

where v represents the weight coefficient of the mixed function, allowing different linear weights to be assigned to the global and local kernel functions. Additionally, determining the optimal kernel parameters is crucial for the model to achieve good learning and generalization capabilities.

2.1.2. Deep Hybrid Kernel Extreme Learning Machine Based on Auto Encoders Concept

Deep learning offers significant advantages in learning and generalization capabilities. In this paper, the concept of auto encoders (AEs) is applied to ELM, resulting in the ELM-AE structure. Multiple ELM-AE layers are stacked to create a deep learning network, which is then enhanced by using hybrid kernel mappings instead of random mappings, forming the DHKELM. The network consists of an input layer, m stacked hidden layers, a hybrid kernel mapping layer, and an output layer. Auto encoders extract features layer by layer, allowing for effective data feature extraction, which enhances the ability to distinguish between easily confused types and improves the accuracy of lithium battery SOH prediction [32,33].

As shown in Figure 1, the integration of the AE concept into the HKELM leads to the construction of the DHKELM model. The specific steps for building the DHKELM model are given below:

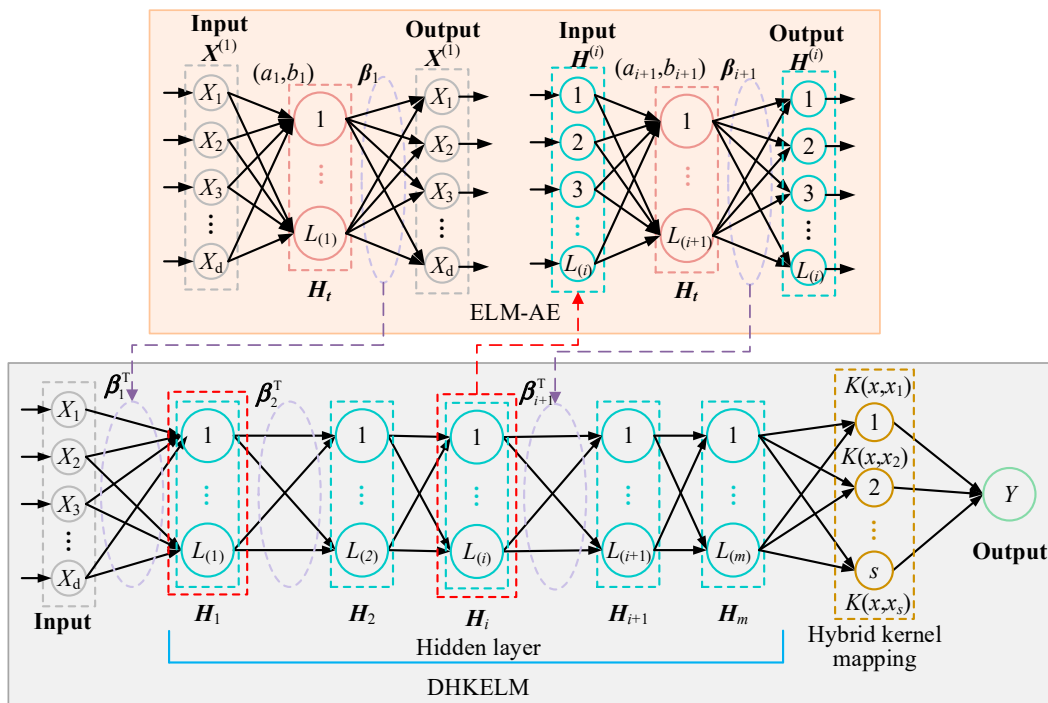


Figure 1. Framework of the DHKELM model.

Step 1: Randomly generate the orthogonal parameters a_i and b_i between the input layer and the hidden layer in the i -th layer of the ELM-AE model.

Step 2: Use the output matrix H_t of the t -th hidden layer as the input for the next layer of the ELM-AE. Subsequently, compute the output H_t and weights β_{i+1} for all the ELM-AE hidden layers, with the update expression given by the following:

$$H_t = \left[\left(\frac{I}{C} + H^T H \right)^{-1} \right]^T \quad (9)$$

$$\beta_{i+1} = \left(\frac{I}{C} + (H_t)^T H_t \right)^{-1} (H_t)^T H_i \quad (10)$$

Step 3: Furthermore, by stacking the hidden layers of the ELM-AE, use the output of the previous layer H_i as the input for the current layer H_{i+1} , thereby constructing a multi-layered architecture:

$$\begin{cases} H_0 = X \\ H_{i+1} = g((\beta_{i+1})^T H_i), i = 0, 1, \dots, m-1 \end{cases} \quad (11)$$

Step 4: The weights and bias parameters of the hybrid kernel mappings layer can be obtained by minimizing the regularized cost function, as shown in Equation (12). These weights and biases are used to map the features processed by the ELM-AE into the output for SOH prediction.

$$Y = g(\omega_{in} H_m + b_{in}) \quad (12)$$

Compared to traditional ELM, DHKELM employs a multi-hidden layer structure that leverages the feature extraction capabilities of AE in deep learning, the generalization and

learning abilities of hybrid kernel functions, and the rapid training advantages of ELM. This combination considerably enhances its capability in SOH prediction.

2.2. The Black-Winged Kite Algorithm and Its Improvements

2.2.1. Black-Winged Kite Algorithm (BKA)

The black-winged kite is a small raptor belonging to the family Accipitridae, widely distributed across open grasslands and farmlands in Europe, Asia, and Africa. Characterized by its black wings, gray-white plumage, and red eyes, it is notable for its capacity to hover at high altitudes while primarily preying on small mammals, birds, and insects, capturing its prey through sudden dives. Inspired by the hunting strategies and migratory patterns of the black-winged kite, an algorithmic model based on the behavioral characteristics of this species has been developed [34]. The principles of the algorithm are as follows:

(1) Initialization

First, similar to most optimization algorithms, the position of each black-winged kite is generated using random initialization:

$$X_i = BK_{lb} + rand(BK_{ub} - BK_{lb}) \quad (13)$$

where i is an integer ranging from 1 to pop, while BK_{lb} and BK_{ub} represent the lower and upper bounds of the j -th dimension of the black kite, respectively. The variable $rand$ is a randomly selected value between $[0, 1]$.

During the initialization phase, the BKA selects the individual with the best fitness value to serve as the leader of the initial population, which is regarded as the optimal position of the black kite. The mathematical representation of the initial leader is as follows, using a minimization problem as an example.

$$f_{best} = \min(f(X_i)) \quad (14)$$

$$X_L = X(find(f_{best} == f(X_i))) \quad (15)$$

where X_L represents the initial leader.

(2) Attack behavior

The hunting behavior of the black-winged kite is renowned for its unique aerial hovering and diving techniques. These birds often remain stationary in the air, using their sharp eyesight to scan the ground for prey, such as small mammals, birds, and insects. Once a target is locked in, the black-winged kite swiftly dives, striking with precision and power. Consequently, the black-winged kite employs two attack strategies during its hunting behavior: one involves soaring and balancing in the air to broadly search for prey, while the other entails more directed circling behavior. Below is the mathematical model representing the attack behavior of the black-winged kite:

$$y_{t+1}^{i,j} = \begin{cases} y_t^{i,j} + n(1 + \sin(r)) \times y_t^{i,j}, & p < r \\ y_t^{i,j} + n \times (2r - 1) \times y_t^{i,j}, & \text{else} \end{cases} \quad (16)$$

$$n = 0.05 \times e^{-2 \times (\frac{t}{T})^2} \quad (17)$$

The variable $y_{t+1}^{i,j}$ represents the position of the i -th black kite at the j -th dimension during the $t + 1$ -th iteration. Here, r is a random number between 0 and 1, p is a constant set at 0.9, T is the total number of iterations, and t is the number of iterations completed so far.

(3) Migration behavior

Bird migration is a complex and efficient collective behavior that typically occurs with seasonal changes, particularly during winter. Many birds migrate from northern regions to southern areas in search of more suitable climates and abundant food resources,

undertaking long-distance flights. This migratory behavior involves not only precise navigation but also coordination and cooperation within the group. Especially during long flights, the selection of leaders is crucial, as it affects the overall efficiency and success rate of migration. In the process of bird migration, the choice of leaders is not fixed; rather, it changes dynamically. Consequently, flocks adjust their leaders flexibly based on specific circumstances during flight, and this dynamic selection mechanism helps maintain the group's flying efficiency.

The authors proposed a hypothesis based on bird migration behavior: when the fitness of the current population falls below that of a randomly selected population, the leader will relinquish their role and integrate into the migrating group, indicating their unsuitability for leading the team. Conversely, if the fitness of the current population exceeds that of the random population, the leader will continue to guide the group forward. This strategy dynamically adjusts the leaders, ensuring that the optimal individuals can successfully lead the group to its destination.

Below is the mathematical model for the migration behavior of the black-winged kite:

$$y_{t+1}^{i,j} = \begin{cases} y_t^{i,j} + C(0, 1) \times (y_t^{i,j} - L_t^j), & F_i < F_{ri} \\ y_t^{i,j} + C(0, 1) \times (L_t^j - m \times y_t^{i,j}), & \text{else} \end{cases} \quad (18)$$

$$m = 2 \times \sin(r + \pi/2) \quad (19)$$

In the equation, L_t^j represents the leading scorer of the j -th dimension of the t -th iteration thus far. F_i denotes the current position of any black-winged kite in the j -th dimension during the t -th iteration, while F_{ri} indicates the fitness value of any black-winged kite at a random position in the j -th dimension during the t -th iteration. $C(0, 1)$ represents the Cauchy mutation, defined as follows:

The one-dimensional Cauchy distribution is a continuous probability distribution characterized by two parameters. Its probability density function is given by the following:

$$f(x, \delta, \mu) = \frac{1}{\pi \delta^2 + (x - \mu)^2}, -\infty < x < \infty \quad (20)$$

when $\delta = 1$ and $\mu = 0$, the probability density function takes on its standard form. The precise formula is as follows:

$$f(x, \delta, \mu) = \frac{1}{\pi} \frac{1}{x^2 + 1}, -\infty < x < \infty \quad (21)$$

2.2.2. Improved Black-Winged Kite Algorithm (IBKA)

The BKA is an emerging population-based optimization technique that mimics the migratory behavior of black-winged kites to tackle complex optimization problems. This algorithm possesses certain capabilities for global search and local exploitation; however, despite its commendable optimization performance across various applications, it still exhibits several notable limitations. Firstly, during the initialization of the population, the algorithm generates individuals randomly, leading to an uneven distribution of solutions throughout a search space. This can result in the population concentrating in specific areas while leaving other regions poorly covered. Such uneven distribution not only diminishes the algorithm's global search ability but may also lead to insufficient population diversity, making it more susceptible to local optima. Secondly, the original algorithm employs an exponential decay function to control the search step size of individuals. While this method gradually reduces the step size with increasing iterations to enhance local search capacity, rapid exponential decay can cause the step size to shrink too quickly, especially in the later stages. This premature reduction limits the algorithm's ability to explore broader regions, often leading to early convergence on suboptimal solutions. Lastly, the migratory behavior simulated by the BKA reflects the collective flight of kites, but the fixed migration step size

lacks randomness and flexibility. As a result, individuals tend to repetitively search local areas, making it difficult to escape local optima, further impacting the algorithm's global search efficiency.

To address these shortcomings, we implemented three improvement strategies: (1) introducing a best point set initialization method to replace the original random initialization during the initialization phase; (2) enhancing the attack behavior using the Gompertz growth model; and (3) improving the migratory behavior through Levy flight strategies.

(1) Best point set initialization

The best point set initialization algorithm creates an initial population that is more evenly distributed throughout the search space. This approach avoids the clustering phenomena that may arise from random initialization, allowing for more comprehensive coverage of the search space. Consequently, it enhances the algorithm's global search capability, accelerates convergence speed, and reduces the uncertainties associated with randomness. Therefore, we have chosen to improve the BKA using the best point set initialization, the principles of which are outlined below.

Let V_d be a unit cube in a d -dimensional space. If $r \in V_d$, the collection of numbers described by Equation (22) can be referred to as the best point set.

$$P_n(k) = \left\{ \left(\left\{ r_1^{(n)} \cdot k \right\}, \left\{ r_2^{(n)} \cdot k \right\}, \dots, \left\{ r_d^{(n)} \cdot k \right\} \right), 1 \leq k \leq n \right\} \quad (22)$$

where the deviation $\varphi(n)$ satisfies $\varphi(n) = C(r, \varepsilon)n^{-1+\varepsilon}$, where $C(r, \varepsilon)n^{-1+\varepsilon}$ is a constant that depends only on r and ε (with ε being any positive number). r represents the best point, $\left\{ r_d^{(n)} \cdot k \right\}$ denotes the fractional part, and n indicates the number of best points, typically set to $r = \{2 \cos(2\pi/p), 1 \leq k \leq d\}$. p is the smallest prime number such that $d \leq (p-3)/2$.

After generating the best point set using Equation (22), it is then mapped into the search space to create the initial population.

(2) Improvement of attack behavior using the Gompertz growth model

In Equation (17), the parameter n regulates the step size for updating an individual's position in the search space, gradually decreasing with the increase in iteration count t to control the algorithm's exploration behavior. Specifically, n is a time-dependent coefficient that reduces the search range through an exponential decay function, allowing the algorithm to have stronger global search capabilities in the early stages while focusing more on local search and fine-tuning in the later stages. However, the exponential decay function used in the original formula may cause the decay rate to be too rapid. As the iteration count t increases, n decreases quickly. This rapid decay can lead to a situation where the algorithm performs a broad global search in the early stages, but the step size shrinks dramatically in the mid to late stages, potentially causing the algorithm to prematurely converge to a local optimum. To address this issue, we replaced the parameter n in Equation (17) with the Gompertz growth model, resulting in a more gradual decay of the step size and balancing the capabilities of the global and local search. This improvement allows the algorithm to transition more smoothly into the local search phase, thereby enhancing the overall performance [35]. The Gompertz growth model is as follows:

$$n = a \times \exp(b \times \exp(ct)) \quad (23)$$

where a represents the asymptote that controls the initial value of the step size; b is the control parameter; and c is the scaling factor that controls the growth rate.

(3) Improvement of migration behavior using Levy flight strategy

The Levy flight strategy is a distribution characterized by infinite variance, which encompasses numerous short-distance jumps and occasional long leaps. This approach allows for detailed exploration during local searches while maintaining the ability to escape from local optima, thus enhancing the overall global search efficiency. By utilizing random jumps of varying lengths, Levy flights can effectively traverse expansive search spaces,

preventing the algorithm from becoming trapped in local optima and ensuring a good balance between exploration and exploitation [36]. Consequently, the Levy flight strategy is introduced into the migration behavior of the BKA. Following this improvement, the modification to Equation (18) is as follows:

$$y_{t+1}^{i,j} = \begin{cases} y_t^{i,j} + C(0, 1) \times (y_t^{i,j} - L_{Levy} L_t^j), F_i < F_{ri} \\ y_t^{i,j} + C(0, 1) \times (L_t^j - m \times y_t^{i,j}), \text{else} \end{cases} \quad (24)$$

$$L_{Levy} = 0.01 \times \frac{\mu \times \sigma}{|v|^{\frac{1}{\beta}}} \quad (25)$$

$$\beta = \frac{1}{1 + e^{\frac{1}{T}}} + 1 \quad (26)$$

$$\sigma = \left(\frac{\Gamma(1 + \beta) \times \sin\left(\frac{\pi\beta}{2}\right)}{\Gamma\left(\frac{1+\beta}{2}\right) \times \beta \times 2^{\left(\frac{\beta-1}{2}\right)}} \right)^{\frac{1}{\beta}} \quad (27)$$

In the equation, μ and σ are random numbers between 0 and 1. The flowchart of the improved algorithm is shown in Figure 2.

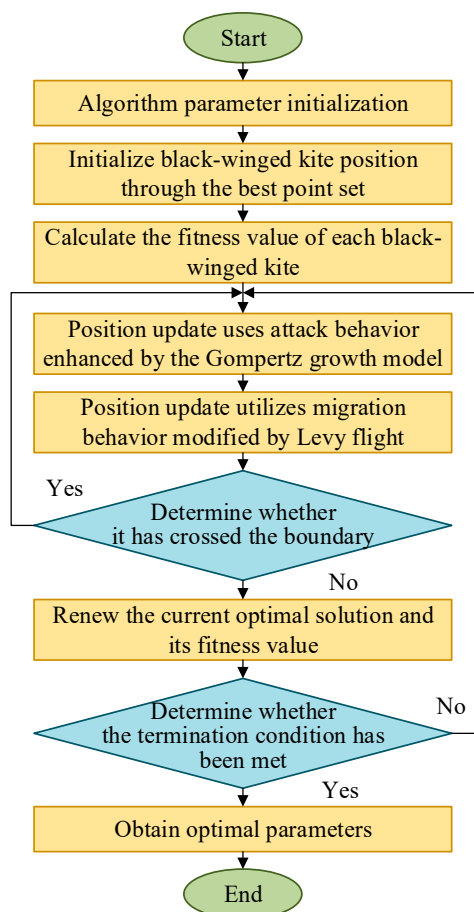


Figure 2. Execution flowchart of the improved black-winged kite algorithm.

2.3. The IBKA-DHKELM Model

To address the shortcomings of traditional ELM in handling non-linear and complex problems, this paper adopts a hybrid kernel method combined with an auto encoder, forming the DHKELM to enhance the model's non-linear fitting ability. However, the

performance of DHKELM still heavily relies on parameter selection, especially the kernel function parameters and model weights. To optimize these key parameters, an IBKA is proposed. Figure 3 depicts a flowchart for SOH prediction using the IBKA-DHKELM combined model, with the following essential steps:

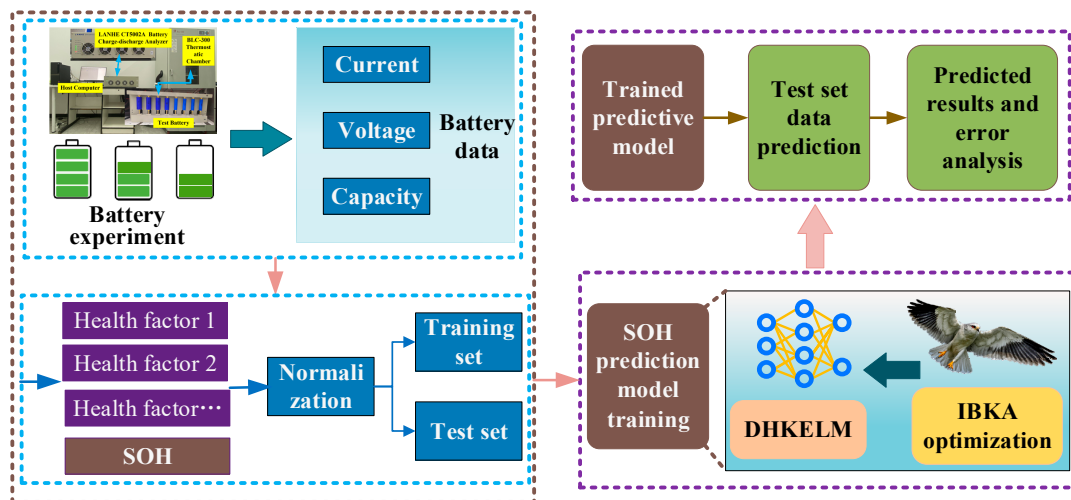


Figure 3. Flowchart of SOH prediction using the IBKA-DHKELM combined model.

(1) Feature Extraction and Data Preprocessing: First, the key features related to battery performance, also known as health indicators, are extracted from the data collected during battery aging experiments. These features include battery capacity and other aging-related metrics. To facilitate analysis and modeling, the battery capacity is converted into the form of SOH. The extracted aging features will serve as inputs to the subsequent model, while the SOH data will serve as the model's output. Next, normalization is performed to eliminate dimensional differences between the different features. Finally, the processed data are divided into training and testing datasets.

(2) Model Parameter Configuration: Based on the battery-related data conditions, appropriate parameters for the IBKA-DHKELM model are set, including the number of iterations, the dimensionality of the optimization parameters, and other relevant settings.

(3) Establish the Fitness Function: The fitness function is constructed using the mean squared error (MSE), as shown in Equation (28).

$$\text{MSE} = \frac{1}{n} \sum_i^n (\hat{y}_i - y_i)^2 \quad (28)$$

where \hat{y}_i represents the predicted value of the SOH, while y_i denotes the actual SOH value.

(4) IBKA Optimizes DHKELM Parameters: A predictive model for DHKELM is established based on the input–output components, and the IBKA optimization algorithm is employed to update the optimal parameters of DHKELM. Instead of using a random distribution to generate the positions of the black-winged kite population, the best point set initialization mapping is used. The fitness values for each black kite in the population are derived based on the fitness function. The positions of the black kites are updated using the improved attack behavior based on the Gompertz growth model and the improved migration behavior based on Levy flights. This process continues iteratively until the maximum number of iterations is reached, resulting in the optimal parameters, which are then used to train the DHKELM model.

(5) SOH Prediction and Validation: First, the trained model is used to make predictions on the test dataset. This process involves inputting the preprocessed test data into the model to generate the corresponding SOH predictions. After obtaining the prediction results, a detailed analysis of these outcomes is necessary. We employ the mean absolute

percentage error (MAPE) and the root mean square error (RMSE) to evaluate the model's predictive performance, with the definitions of both errors provided below.

$$\text{MAPE} = \frac{1}{n} \sum_i^n \left| \frac{\hat{y}_i - y_i}{y_i} \right| \times 100\% \quad (29)$$

$$\text{RMSE} = \sqrt{\frac{1}{n} \sum_i^n (\hat{y}_i - y_i)^2} \quad (30)$$

Smaller MAPE and RMSE values indicate more accurate predictions.

3. Experimental Dataset and Feature Extraction

3.1. Dataset

This study utilizes two distinct datasets: dataset A, which consists of lithium battery aging data obtained from NASA's Prognostics Center of Excellence (PCoE), and dataset B, which is derived from the lithium-ion battery dataset at the Center for Advanced Life Cycle Engineering (CALCE) at the University of Maryland [17].

Dataset A comprises data from four batteries, B5, B6, B7, and B18. The four batteries are 18,650 lithium-ion cells with a nominal capacity of 2 Ah, subjected to charge–discharge aging tests. The experiments for all the batteries were conducted at 24 °C using constant current–constant voltage (CC–CV) cycling tests. Initially, a constant current of 1.5 A was applied to charge the batteries until the voltage reached 4.2 V. Subsequently, charging continued in the constant voltage mode until the charging current dropped below 20 mA. The discharge tests were conducted using a constant current of 2 A until the voltages of batteries B5, B6, B7, and B18 decreased to their cutoff voltages of 2.7 V, 2.5 V, 2.2 V, and 2.5 V, respectively.

Dataset B includes four batteries, CS35, CS36, CS37, and CS38. The cathode material for these batteries is lithium cobalt oxide (LiCoO₂), with a nominal capacity of 1.1 Ah. In a 24 °C environment, they were charged at a rate of 0.5 C using CC until the battery voltage reached 4.2 V. Charging continued in the constant voltage mode until the charging current fell to 50 mA. The discharge tests were carried out under a constant current output mode of 1 C until the voltage dropped to 2.7 V.

The capacity degradation curves for both datasets are shown in Figure 4. As illustrated, the capacity degradation curves exhibit strong non-linearity and non-stationarity, influenced by factors such as capacity recovery.

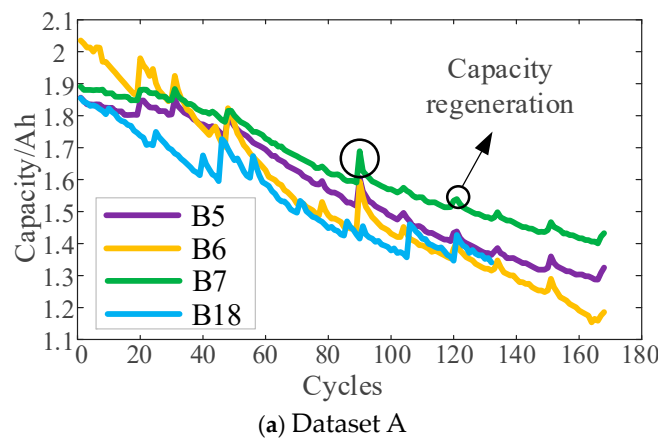


Figure 4. Cont.

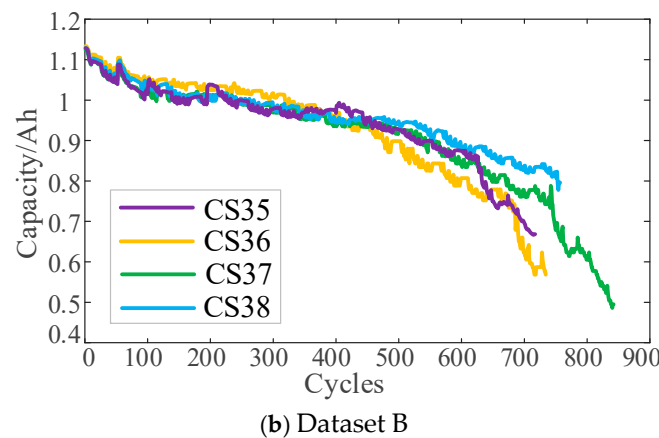


Figure 4. Battery capacity degradation curve.

3.2. Feature Extraction

Aging features, also known as health factors, refer to various characteristics that reflect the aging state of a battery, such as voltage, current, and temperature [37]. Generally, capacity can directly indicate the health status of a battery; however, in practice, measuring battery capacity can be challenging. Thus, the role of health factors becomes particularly crucial. By analyzing historical data on battery health factors, a health model can be established to predict the battery's health status, providing a basis for maintenance and replacement decisions [38]. The charge–discharge curves of the batteries at different cycle counts are illustrated in Figure 5.

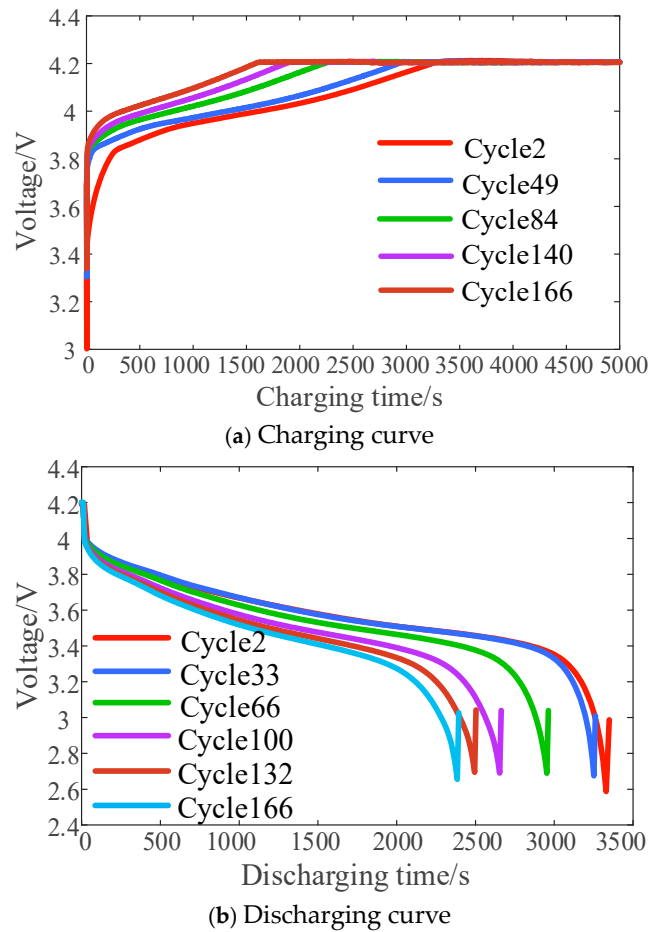


Figure 5. Charging and discharging curve of batteries.

From Figure 5a, it can be observed that the second cycle requires the longest charging time, while the 166th cycle requires the shortest charging time. As the charge–discharge cycle count increases, the charging time during the CC phase gradually decreases. This indicates that the charging voltage in the CC phase contains implicit characteristics of battery performance degradation, which can indirectly represent the battery's health status. Similarly, Figure 5b shows that the discharge voltage also reveals characteristics of battery performance degradation and can likewise serve as an indirect indicator of the battery's health status [39].

In the experiment, considering the correlation between health factors and SOH as well as the difficulty in extracting health factors, four key parameters were ultimately extracted from the charge–discharge data: time of equal voltage rise, time of equal voltage drop, constant current charging time, and constant voltage charging time. These parameters were designated as F1, F2, F3, and F4, respectively. The curves of the four health factors extracted from the data of battery B5 are shown in Figure 6.

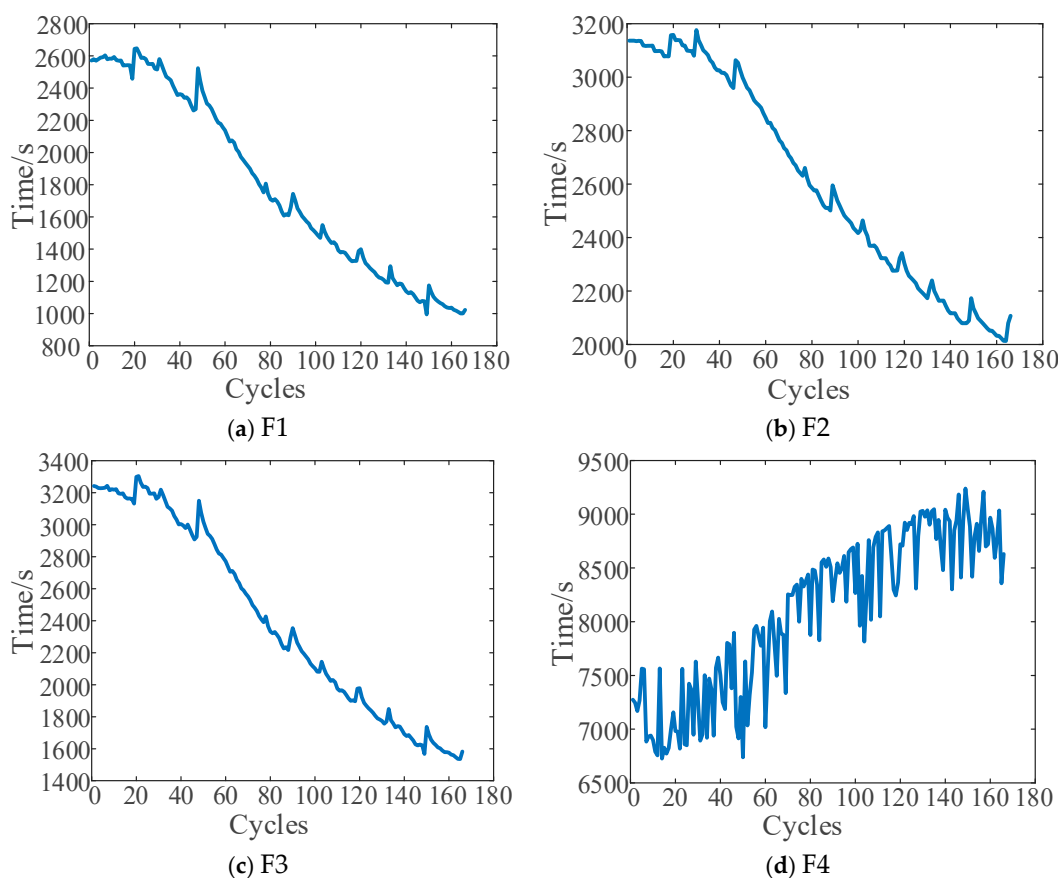


Figure 6. Health factors of battery B5.

4. Experimental Results and Analysis

To validate the effectiveness and superiority of the proposed IBKA-DHKELM model, it was applied to SOH prediction for dataset A and dataset B. The parameters requiring optimization in the DHKELM model include the number of nodes in each hidden layer, kernel weight coefficients, penalty coefficients, regularization coefficients, and kernel parameters. For batteries B5 and B18 in dataset A, 40% of the data from the batteries was selected as the training set, with the remaining 60% used as the testing set. The results were then compared with three predictive models: ELM, DHKELM, and BKA-DHKELM. The SOH prediction results for the two battery groups in dataset A using different algorithms are presented in Figures 7 and 8, with the corresponding errors detailed in Table 1.

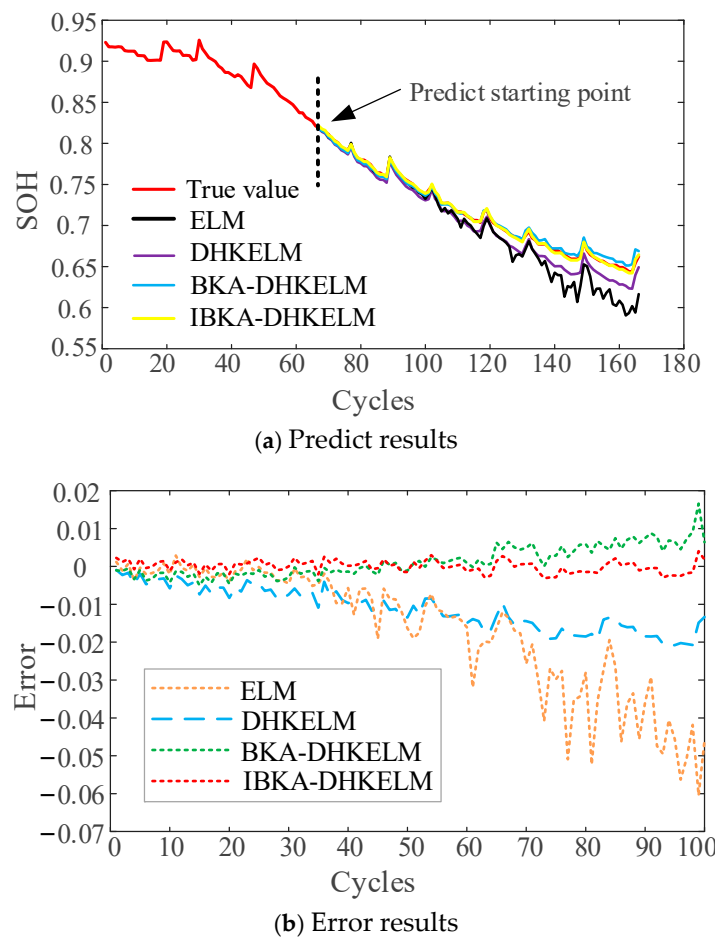


Figure 7. SOH prediction results and errors of battery B5.

From Figures 7 and 8, it is evident that there are significant differences in the prediction performance of the various models. Among the two batteries, the best prediction results were obtained using the IBKA-DHKELM model, followed by BKA-DHKELM, DHKELM, and finally ELM, which performed the worst. For example, in Figure 7a, the ELM model shows the poorest results, particularly in the later stages where the prediction errors gradually increase, and the prediction curve appears irregular, indicating that it fails to adequately extract the features from the data. The DHKELM model shows a noticeable improvement over ELM, reducing errors but still falling short of the ideal prediction accuracy. The BKA-DHKELM model benefits from the optimization provided by the BKA, resulting in further enhancement of prediction performance, although it still has limitations. In contrast, the IBKA-DHKELM model demonstrates superior performance, significantly improving the prediction accuracy through the optimized hyperparameters of the IBKA, with the predictions closely aligning with the actual values.

From Table 1, it is evident that there are significant differences in prediction errors among the various models for the two battery groups. Compared to the ELM and DHKELM models, both the BKA-DHKELM and IBKA-DHKELM models show substantial improvements in the MAPE and RMSE metrics, with the IBKA-DHKELM model demonstrating the highest prediction accuracy. Taking the B5 battery as an example, the RMSE for the ELM model is 0.0235, indicating a relatively large prediction error. The DHKELM model shows an RMSE of 0.0125, which is a 46.8% improvement in the prediction accuracy compared to the ELM model. The BKA-DHKELM model further reduces the RMSE to 0.0042, resulting in a 66.4% enhancement in prediction accuracy. The IBKA-DHKELM model achieves an RMSE of only 0.0015, representing improvements of 64.3%, 88.0%, and 93.6% compared to the BKA-DHKELM, DHKELM, and ELM models, respectively. Thus, the proposed

IBKA-DHKELM model can accurately predict changes in SOH, achieving a higher level of prediction precision.

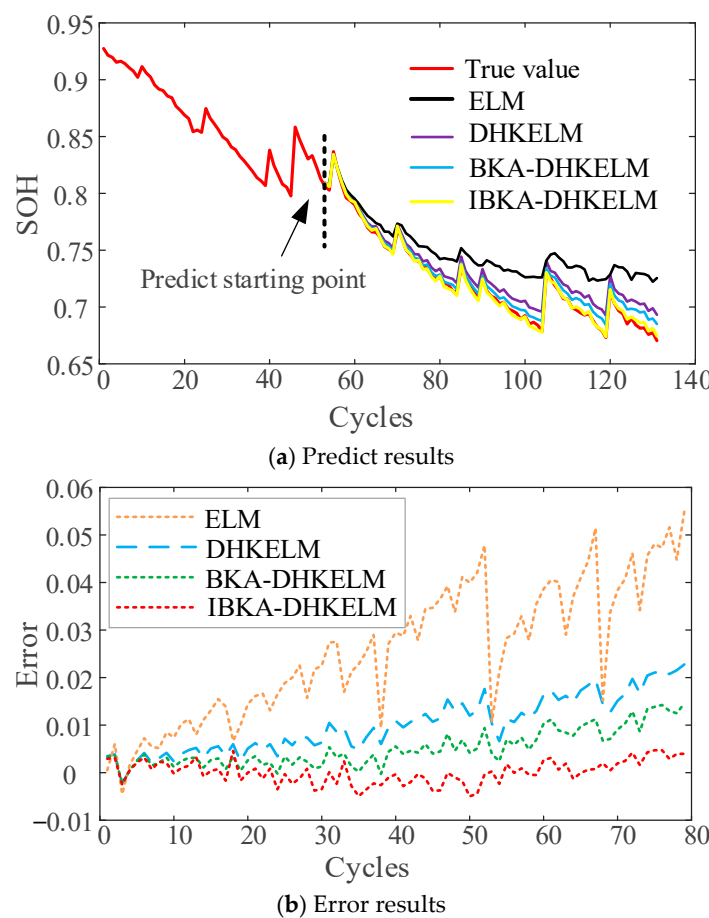


Figure 8. SOH prediction results and errors of battery B18.

Table 1. Comparison of errors from different algorithms for batteries B5 and B18.

No	Model	MAPE/%	RMSE
B5	ELM	2.50	0.0235
	DHKELM	1.63	0.0125
	BKA-DHKELM	0.47	0.0042
	IBKA-DHKELM	0.18	0.0015
B18	ELM	3.66	0.0294
	DHKELM	1.44	0.0117
	BKA-DHKELM	0.75	0.0065
	IBKA-DHKELM	0.28	0.0024

To validate the robustness of the proposed method in handling inconsistencies between different individual cells within the same dataset, the IBKA-DHKELM model was applied for SOH prediction on batteries B6 and B7. The first 40% of the data was used as the training set, while the remaining 60% served as the test set. The SOH prediction results for both cells are displayed in Figure 9. As shown in the figure, the IBKA-DHKELM model achieved strong predictive performance for both cells, with an R^2 of 0.9974 for each. However, the error histograms reveal that the prediction errors for cell B6 are more concentrated near zero compared to those for cell B7, indicating a closer alignment with the actual values.

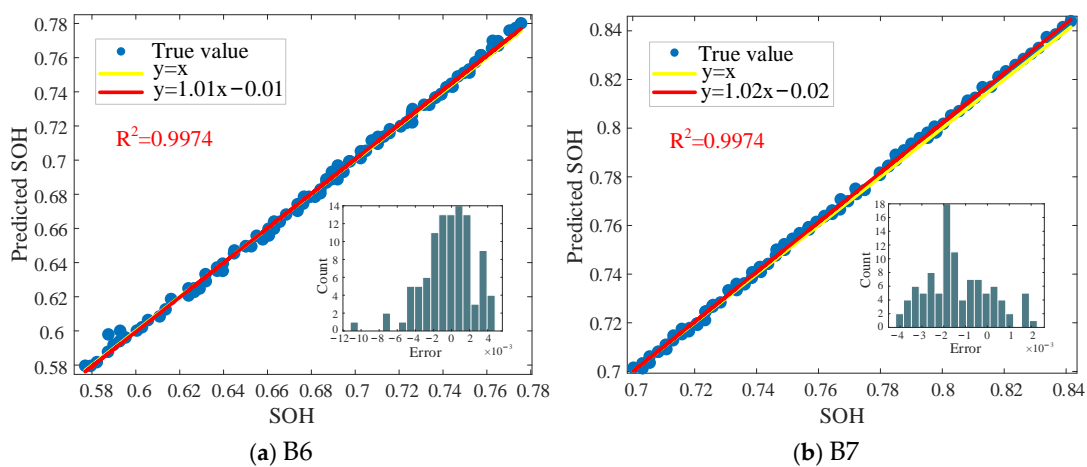


Figure 9. SOH prediction results of batteries B6 and B7.

To validate the generalizability and stability of the proposed IBKA-DHKELM model, we conducted training and prediction on a new battery dataset, dataset B. This step ensures that the model not only performs well on specific data but can also handle different types of battery data. By training the model on a completely new dataset, we effectively test its adaptability and ensure that it maintains a high prediction accuracy on unseen data. We applied four prediction models—ELM, DHKELM, BKA-DHKELM, and IBKA-DHKELM—to predict the SOH for the CS35 and CS36 batteries in dataset B. The training dataset for both battery groups consisted of the first 40% of the total data, while the remaining 60% was used as a test set for validation. The SOH prediction results for the four models are illustrated in Figures 10 and 11, with the corresponding errors summarized in Table 2.

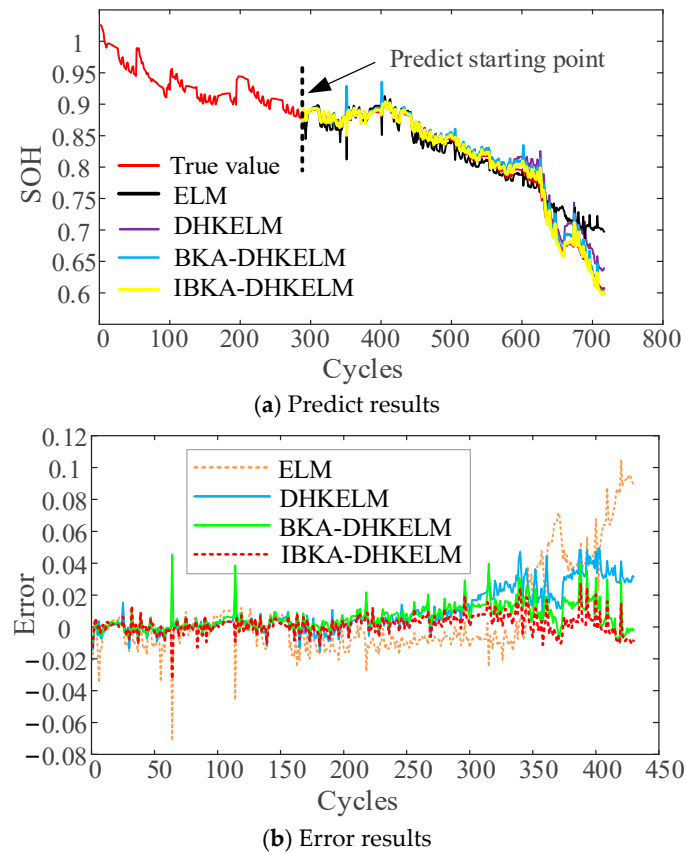


Figure 10. SOH prediction results and errors of battery CS35.

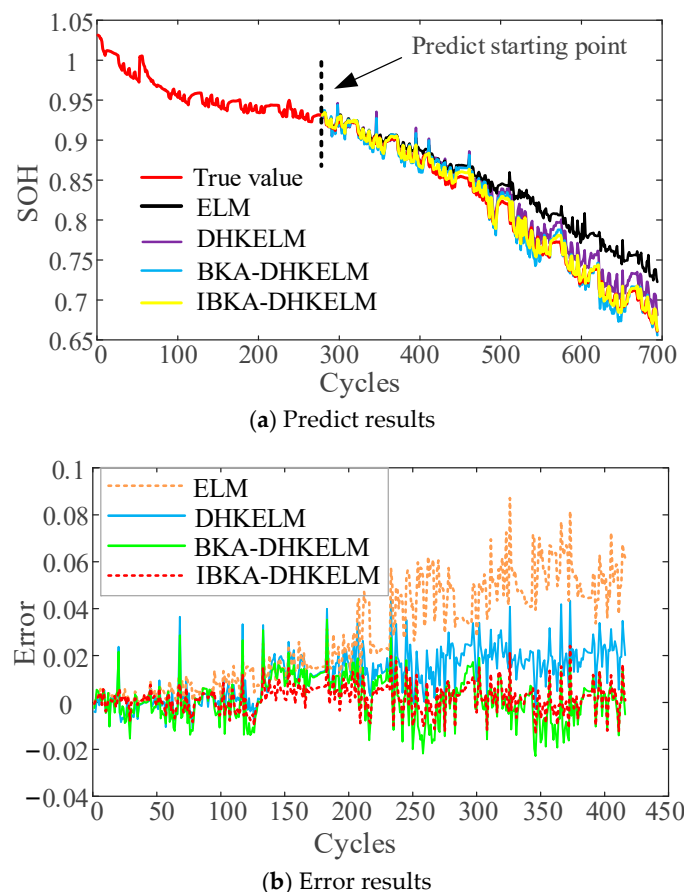


Figure 11. SOH prediction results and errors of battery CS36.

Table 2. Comparison of prediction errors for batteries CS35 and CS36 using different algorithms.

No	Model	MAPE/%	RMSE
CS35	ELM	2.47	0.0279
	DHKELM	1.61	0.0170
	BKA-DHKELM	0.94	0.0101
	IBKA-DHKELM	0.57	0.0062
CS36	ELM	3.80	0.0358
	DHKELM	1.70	0.0161
	BKA-DHKELM	0.95	0.0095
	IBKA-DHKELM	0.58	0.0060

From Figures 10 and 11, it can be seen that the trends of the various algorithms are generally consistent across the CS35 and CS36 battery models. The ELM model performed the worst, while the DHKELM model showed significant improvement over the ELM. The BKA-DHKELM further reduced the error, with the best performance observed in the IBKA-DHKELM model. As shown in Table 2, for the prediction errors of the CS35 battery, the RMSE of the ELM model was 0.0279, indicating a relatively large error. The RMSE of the DHKELM model improved to 0.0170, enhancing the prediction accuracy by 39.1%. The RMSE of the BKA-DHKELM model was 0.0101, representing a further improvement of 40.6% compared to DHKELM. Finally, the RMSE of the IBKA-DHKELM model was 0.0062, which signifies increases in the prediction accuracy of 38.6%, 63.5%, and 77.8% over the BKA-DHKELM, DHKELM, and ELM models, respectively.

Similarly, to validate the robustness of the proposed method regarding battery inconsistencies, the IBKA-DHKELM model was applied to predict the SOH for batteries CS37 and CS38. The first 40% of the data was used as the training set, and the prediction

results are illustrated in Figure 12. As shown in the figure, the IBKA-DHKELM model demonstrates strong predictive performance for both cells.

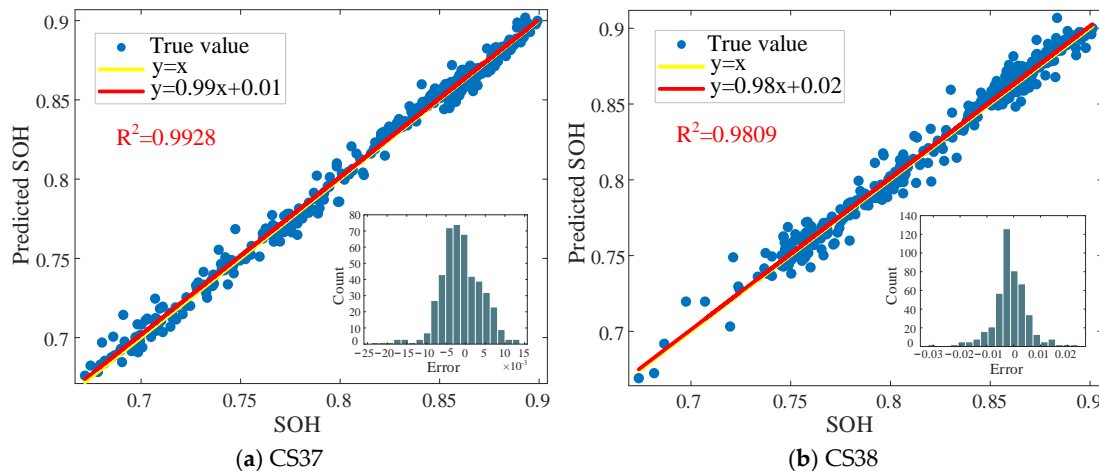


Figure 12. SOH prediction results of batteries CS37 and CS38.

To further validate the performance of the model established in this paper, a comparison was made between the GBLS Booster, IQPSO-LSTM, EMD-GRU-ARIMA, and Encoder-TCN advanced models in predicting the SOH on B5. The SOH prediction results for the different methods are shown in Table 3. Compared with the other methods in the literature, the precision of the method presented in this paper exceeds that of most other methods.

Table 3. SOH prediction results of different methods.

No	Models	Training Set Ratio	RMSE
B5	GBLS Booster [40]	42%	0.0097
	IQPSO-LSTM [41]	50%	0.0065
	EMD-GRU-ARIMA [42]	60%	0.0060
	Encoder-TCN [43]	50%	0.0060
	IBKA-DHKELM	40%	0.0015

In summary, the IBKA-DHKELM model outperformed other algorithms in predicting battery SOH, achieving the lowest MAPE and RMSE. The introduction of the improved black-winged kite algorithm, along with the use of auto encoders and hybrid kernel functions, has significantly enhanced the predictive performance of the model. These results demonstrate that IBKA-DHKELM not only improves the accuracy of SOH predictions but also exhibits strong generalization ability, making it suitable for different types of battery data.

5. Conclusions

To enhance the accuracy and robustness of SOH prediction for lithium batteries, an IBKA-DHKELM predictive model has been proposed. The main conclusions of this study are as follows:

1. The incorporation of auto encoders and hybrid kernel functions has improved the DHKELM model, enhancing its feature differentiation and non-linear mapping capabilities, which in turn increases the accuracy of SOH predictions for lithium batteries.
2. The improved black-winged kite algorithm overcomes the shortcomings of the BKA, providing optimal parameters for the DHKELM model, and significantly enhancing both the SOH prediction accuracy and stability.
3. The experimental results from the two different types of batteries from NASA and the University of Maryland demonstrate that the IBKA-DHKELM model achieves

excellent predictive accuracy and stability. Compared to the ELM, DHKELM, and BKA-DHKELM methods, the proposed approach outperforms the others in all the metrics. Additionally, this method can be applied for offline training and online SOH prediction for lithium batteries. Therefore, the proposed method represents a high-accuracy, robust, and straightforward approach to SOH prediction.

Future research will focus on extracting features under variable charge and discharge currents, optimizing feature extraction methods, enhancing the model's real-time application capabilities, and expanding its use in multi-variable environments, all aimed at further improving the accuracy and reliability of lithium-ion battery SOH prediction.

Author Contributions: Conceptualization, J.F. and Z.S.; methodology, J.F.; software, J.M.; validation, J.M.; formal analysis, J.F.; investigation, Z.S.; resources, J.M.; data curation, Z.S.; writing—original draft preparation, J.F.; writing—review and editing, C.W. and Z.S.; supervision, J.M.; project administration, J.F.; funding acquisition, J.M. and Z.S. All authors have read and agreed to the published version of the manuscript.

Funding: This work was supported by the Xinjiang Uygur Autonomous Region Key R&D Program under Grant (2022B01019-2), the Key Research and Development Program of Shaanxi Province under Grant (2024GX-YBXM-442), and the Fundamental Research Funds for the Central Universities under Grant (xxj032023002).

Data Availability Statement: Data will be made available upon request.

Conflicts of Interest: The authors declare no conflicts of interest.

References

- Zhou, L.; Lai, X.; Li, B.; Yao, Y.; Yuan, M.; Weng, J.H.; Zheng, Y.J. State Estimation Models of Lithium-Ion Batteries for Battery Management System: Status, Challenges, and Future Trends. *Batteries* **2023**, *9*, 131. [[CrossRef](#)]
- Zhang, S.; Wang, X.; Li, C.; Xiao, D. In Robust State of Charge Estimation for Battery with Self-Adaptive Super Twisting Sliding Mode Observer. In Proceedings of the IECON 2023—49th Annual Conference of the IEEE Industrial Electronics Society, Singapore, 16–19 October 2023; pp. 1–6.
- Dini, P.; Colicelli, A.; Saponara, S. Review on Modeling and SOC/SOH Estimation of Batteries for Automotive Applications. *Batteries* **2024**, *10*, 34. [[CrossRef](#)]
- Meng, J.; Ricco, M.; Luo, G.; Swierczynski, M.; Stroe, D.I.; Stroe, A.I.; Teodorescu, R. An Overview and Comparison of Online Implementable SOC Estimation Methods for Lithium-Ion Battery. *IEEE Trans. Ind. Appl.* **2018**, *54*, 1583–1591. [[CrossRef](#)]
- Yang, Z.; Song, Z.; Meng, J.; Zheng, K. SOH Evaluation Method for LFP Energy Storage System Based on Cell-to-module Transfer. *High Volt. Eng.* **2023**, *49*, 4142–4149.
- Sun, X.W.; Zhang, Y.; Zhang, Y.C.; Wang, L.C.; Wang, K. Summary of Health-State Estimation of Lithium-Ion Batteries Based on Electrochemical Impedance Spectroscopy. *Energies* **2023**, *16*, 5682. [[CrossRef](#)]
- Qin, Q.; Zhao, S.; Chen, S.W.; Huang, D.S.; Liang, J. Adaptive and robust prediction for the remaining useful life of electrolytic capacitors. *Microelectron. Reliab.* **2018**, *87*, 64–74. [[CrossRef](#)]
- Chang, Y.; Fang, H.J. A hybrid prognostic method for system degradation based on particle filter and relevance vector machine. *Reliab. Eng. Syst. Saf.* **2019**, *186*, 51–63. [[CrossRef](#)]
- He, N.; Yang, Z.; Qian, C. SOH estimation of lithium-ion battery based on non-parametric model and particle filter. *J. Electron. Meas. Instrum.* **2024**, *38*, 148–159.
- Chen, Y.; He, Y.G.; Li, Z.; Chen, L.P.; Zhang, C.L. Remaining Useful Life Prediction and State of Health Diagnosis of Lithium-Ion Battery Based on Second-Order Central Difference Particle Filter. *IEEE Access* **2020**, *8*, 37305–37313. [[CrossRef](#)]
- Qi, N.; Yan, K.; Yu, Y.J.; Li, R.; Huang, R.; Chen, L.; Su, Y.F. Machine learning and neural network supported state of health simulation and forecasting model for lithium-ion battery. *Front. Energy* **2024**, *18*, 223–240. [[CrossRef](#)]
- Shen, J.; He, Y.; Ma, Z. Progress of model based SOC and SOH estimation methods for lithium-ion battery. *CIESC J.* **2018**, *69*, 309–316.
- Zhang, S.; Wang, X.; Chen, Z.; Xiao, D. Anti-disturbance State-of-Charge Estimation for Lithium-ion Batteries Using Nonlinear Extended State Observers. *IEEE Trans. Transp. Electrif.* **2024**, *1*. [[CrossRef](#)]
- Jin, S.; Dong, J. Review on progress of data-driven based health state estimation for lithium-ion batteries. *Chin. J. Sci. Instrum.* **2024**, *45*, 45–59.
- Zhao, J.H.; Zhu, Y.; Zhang, B.; Liu, M.Y.; Wang, J.X.; Liu, C.H.; Hao, X.W. Review of State Estimation and Remaining Useful Life Prediction Methods for Lithium-Ion Batteries. *Sustainability* **2023**, *15*, 5014. [[CrossRef](#)]
- Fu, J.; Wu, C.; Wang, J.; Haque, M.M.; Geng, L.; Meng, J. Lithium-ion battery SOH prediction based on VMD-PE and improved DBO optimized temporal convolutional network model. *J. Energy Storage* **2024**, *87*, 111392. [[CrossRef](#)]

17. Wang, Y.; Ni, Y.; Zheng, Y.; Shi, X.; Wang, J. Remaining Useful Life Prediction of Lithium-ion Batteries Based on Support Vector Regression Optimized and Ant Lion Optimizations. *Proc. Chin. Soc. Electr. Eng.* **2021**, *41*, 1445–1457.
18. Mawonou, K.S.R.; Eddahetch, A.; Dumur, D.; Beauvois, D.; Godoy, E. State-of-health estimators coupled to a random forest approach for lithium-ion battery aging factor ranking. *J. Power Sources* **2021**, *484*, 14. [[CrossRef](#)]
19. Wen, J.P.; Chen, X.; Li, X.H.; Li, Y.K. SOH prediction of lithium battery based on IC curve feature and BP neural network. *Energy* **2022**, *261*, 8. [[CrossRef](#)]
20. Dai, H.D.; Wang, J.X.; Huang, Y.Y.; Lai, Y.; Zhu, L.Q. Lightweight state-of-health estimation of lithium-ion batteries based on statistical feature optimization. *Renew. Energy* **2024**, *222*, 13. [[CrossRef](#)]
21. Xu, J.; Ni, Y.; Zhu, C. Remaining Useful Life Prediction for Lithium-Ion Batteries Based on Improved Support Vector Regression. *Trans. China Electrotech. Soc.* **2021**, *36*, 3693–3704.
22. Li, Y.; Kan, H.; Guo, Z.; Wang, D.; Wang, C. Prediction of Remaining Useful Life of Lithium-Ion Battery Based on Data Preprocessing and VMD-LSTM-GPR. *Trans. China Electrotech. Soc.* **2024**, *39*, 3244–3258.
23. Nakano, K.; Vögler, S.; Tanaka, K. Advancing state of health estimation for electric vehicles: Transformer-based approach leveraging real-world data. *Adv. Appl. Energy* **2024**, *16*, 18. [[CrossRef](#)]
24. Zhang, C.; Zhao, S.; He, Y. State-of-health Estimate for Lithium-ion Battery Using Information Entropy and PSO-LSTM. *J. Mech. Eng.* **2022**, *58*, 180–190.
25. Mao, L.; Wen, J.; Zhao, J.; Dong, H. Joint estimation of SOC and SOH at lithium-ion battery charging cut-off voltage based on an ensemble extreme learning machine. *Power Syst. Prot. Control.* **2023**, *51*, 86–95.
26. Song, J.; Liu, Y.; Cui, L.; Zhang, M. Remaining Useful Life Prediction of Lithium-ion Batteries Based on Improved Grey Wolf Optimization Multiple Kernel Extreme Learning Machine. *J. Power Supply* **2023**, *21*, 168–176.
27. Zhang, Y.D.; Ma, H.Y.; Wang, S.; Li, S.Y.; Guo, R. Indirect prediction of remaining useful life for lithium-ion batteries based on improved multiple kernel extreme learning machine. *J. Energy Storage* **2023**, *64*, 12. [[CrossRef](#)]
28. Zhang, Z.; Wang, X.; Yue, Y. Heuristic Optimization Algorithm of Black-Winged Kite Fused with Osprey and Its Engineering Application. *Biomimetics* **2024**, *9*, 595. [[CrossRef](#)]
29. Haohao, M.; As'arry, A.; Yanwei, F.; Lulu, C.; Delgoshaei, A.; Ismail, M.I.S.; Ramli, H.R. Improved black-winged kite algorithm and finite element analysis for robot parallel gripper design. *Adv. Mech. Eng.* **2024**, *16*. [[CrossRef](#)]
30. Zhu, J.; Tan, T.; Wu, L.; Yuan, H. RUL Prediction of Lithium-Ion Battery Based on Improved DGWO-ELM Method in a Random Discharge Rates Environment. *IEEE Access* **2019**, *7*, 125176–125187. [[CrossRef](#)]
31. Zhao, Q.; Cai, Y.; Wang, X. Remaining Useful Life Prediction for Full Life Cycle of Lithium-ion Battery. *J. Power Supply* **2024**, *22*, 197–204.
32. Wang, C.; Lin, H.; Pang, X. Short-term photovoltaic power combination prediction based on HPO-VMDAND MISMA-DHKELM. *Acta Energiae Solaris Sin.* **2023**, *44*, 65–73.
33. Shang, L.; Huang, C.; Hou, Y.; Li, H.; Hui, Z.; Zhang, J. Short-Term Wind Power Prediction by Using the Deep Kernel Extreme Learning Machine with Well-Selected and Optimized Features. *J. Xi'an Jiaotong Univ.* **2023**, *57*, 66–77.
34. Wang, J.; Wang, W.C.; Hu, X.X.; Qiu, L.; Zang, H.F. Black-winged kite algorithm: A nature-inspired meta-heuristic for solving benchmark functions and engineering problems. *Artif. Intell. Rev.* **2024**, *57*, 53. [[CrossRef](#)]
35. Chauhan, P.; Pant, M.; Deep, K. Gompertz PSO variants for Knapsack and Multi-Knapsack Problems. *Appl. Math.-J. Chin. Univ. Ser. B* **2021**, *36*, 611–630. [[CrossRef](#)]
36. Zhang, B.; Liu, W.; Cai, Y.; Zhou, Z.; Wang, L.; Liao, Q.; Fu, Z.; Cheng, Z. State of health prediction of lithium-ion batteries using particle swarm optimization with Levy flight and generalized opposition-based learning. *J. Energy Storage* **2024**, *84*, 110816. [[CrossRef](#)]
37. Xu, H.W.; Wu, L.F.; Xiong, S.Z.; Li, W.; Garg, A.; Gao, L. An improved CNN-LSTM model-based state-of-health estimation approach for lithium-ion batteries. *Energy* **2023**, *276*, 11. [[CrossRef](#)]
38. Lin, M.Q.; Wu, D.G.; Meng, J.H.; Wang, W.; Wu, J. Health prognosis for lithium-ion battery with multi-feature optimization. *Energy* **2023**, *264*, 10. [[CrossRef](#)]
39. Jiang, Y.Y.; Chen, Y.; Yang, F.F.; Peng, W.W. State of health estimation of lithium-ion battery with automatic feature extraction and self-attention learning mechanism. *J. Power Sources* **2023**, *556*, 14. [[CrossRef](#)]
40. Yang, P.; Yang, H.D.; Meng, X.B.; Song, C.R.; He, T.L.; Cai, J.Y.; Xie, Y.Y.; Xu, K.K. Joint evaluation and prediction of SOH and RUL for lithium batteries based on a GBLS booster multi-task model. *J. Energy Storage* **2024**, *75*, 109741. [[CrossRef](#)]
41. Peng, S.; Sun, Y.; Liu, D.; Yu, Q.; Kan, J.; Pecht, M. State of health estimation of lithium-ion batteries based on multi-health features extraction and improved long short-term memory neural network. *Energy* **2023**, *282*, 128956. [[CrossRef](#)]
42. Liu, Z.; Zhang, Z.; Guo, L.; Meng, H.; Liu, X. State of Health Prediction for Lithium-ion Batteries Based on Empirical Mode Decomposition. *J. Mech. Eng.* **2024**, *60*, 272–281.
43. Zhang, X.; Zhang, J.; Jiang, Y. Power battery health evaluation based on improved TCN model. *Energy Storage Sci. Technol.* **2022**, *11*, 1617–1626.